# A method to ingest GPS-TEC into the NeQuick ionospheric model

C. Brunini,[1,2] E. Gularte,[1,2] A. Meza,[1,2] S. M. Radicella,[3] B. Nava,[3] P. Coisson,[3] and M. Mosert[1,4]

[1]   This paper presents a method to ingest Total Electron Content measurements from ground-based GPS receivers into the empirical NeQuick model. The method here presented relies upon optimizing the parameter that primarily drives the NeQuick profile, i.e., the electron density of the F2 peak, $N_mF2$. The effectiveness of the method is assessed in a rather benevolent ionospheric scenario: a midlatitude region and quiet geomagnetic days that cover solstices and equinoxes conditions during a medium-high solar activity year. Thus, the procedure demonstrated to be capable of improving the climatological value of $N_mF2$ computed from the Radioscience Section of the International Telecommunication Union (ITU-R) database. This capability was assessed by comparing the ITU-R value and the corrected value produced by our method to the value measured with a Digisonde. The result of this comparison was an overall reduction of the error of the $N_mF2$ parameter to approximately half of its original value.

**Citation:**   Brunini, C., E. Gularte, A. Meza, S. M. Radicella, B. Nava, P. Coisson, and M. Mosert (2007), A method to ingest GPS-TEC into the NeQuick ionospheric model, *Radio Sci.*, *42*, RS4013, doi:10.1029/2006RS003521.

## 1. Introduction

[2]   During the last years the possibility to estimate ionopsheric parameters using GPS observations has opened a very active and promising field of research. Dual-frequency GPS observations provide information on the integrated electron density along the raypath of the signals from the satellites to the receivers and hence GPS is primarily used to estimate the total electron content (TEC). There are today a variety of approaches for processing GPS observations and producing maps of the vertical TEC (VTEC) distribution with high spatial and temporal resolution [e.g., *Gao et al.*, 1994; *Feltens*, 1998; *Mannucci et al.*, 1998; *Hernández-Pajares et al.*, 1999; *Schaer*, 1999]. Many of these studies have been possible thanks to the existence of a worldwide network of GPS receivers that operates under the umbrella of the International Global Navigation Satellite Systems Service (IGS) [*Beutler et al.*, 1999; *Hernández-Pajares*, 2003].

[3]   The radial geometry of GPS observations collected from ground-based receivers limits their capability to provide information on the vertical distribution of the electron density. *Hajj et al.* [1994], *Howe et al.* [1998], *Meza et al.* [2000], among others, used simulated data to demonstrate that this limitation can be overcome by adding observations collected from the space by GPS receivers flying onboard of low-Earth orbiting (LEO) satellites (e.g., GPS-Met, CHAMP, GRACE, SAC-C, TOPEX/Poseidon, Jason 1, etc.). Raypaths from the higher GPS to a LEO satellite provide the TEC at different heights through the ionosphere, thus allowing to estimate the vertical distribution of the electron density. In addition, *Ruffini et al.* [1999], *Hernández-Pajares et al.* [2000], *Jakowski et al.* [2002], *García-Fernández et al.* [2003], among others, demonstrated the capability to estimate the actual vertical electron distribution by means of tomographic processing strategies that make use of space-based GPS observations.

[4]   In previous works [*Meza*, 1999; *Brunini et al.*, 2003], we presented a method to estimate the three-dimensional (latitude, longitude and time) VTEC distribution, as well as the four-dimensional (including height) electron density distribution, using ground-based GPS observations belonging to the IGS network and space-based GPS observations collected by the NASA's GPS-Met mission. We used a nontomographic approach based on an Oxygen Chapman profile to represent the vertical distribution of the electron density. Then, we adjusted the

[1]Consejo Nacional de Investigaciones Científicas y Tecnológicas, Buenos Aires, Argentina.
[2]Facultad de Ciencias Astronómicas y Geofísicas, Universidad Nacional de La Plata, Buenos Aires, Argentina.
[3]Aeronomy and Radiopropagation Laboratory, Abdus Salam International Center for Theoretical Physics, Trieste, Italy.
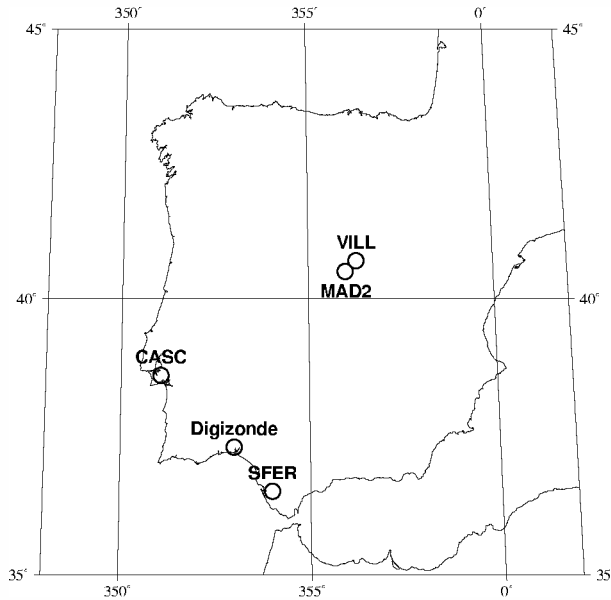[4]Complejo Astronómico El Leoncito, San Juan, Argentina.

**Figure 1.** Location of the GPS receivers and the Digisonde in the Peninsular Spain.

electron density of the peak of the profile in order to minimize the differences between the TEC measured by GPS and computed by integration of the electron density described by the Chapman approach. On the other hand, *Komjathy et al.* [1998], *Hernández-Pajares et al.* [2002], *Nava et al.* [2003], *Hajj et al.* [2004], among others, discussed different nontomographic approaches that rely upon different empirical models of the ionosphere and make use of different strategies to ingest GPS data into those models.

[5] In this contribution we present a new procedure in which the rather simple Chapman approach, commonly used as a standard model, is replaced by the more complex but realistic NeQuick model [*Radicella and Leitinger*, 2001]. The method is not intended to be an improvement over the tomographic approach; rather, is to be viewed as a device to improve the mean parameter of a ionospheric model (the NeQuick model in our case) by means of GPS data, so as to better understand the underlying physics. A good model would allow us to obtain TEC values where data is not available, contrary to the tomographic method, which bases its predictions on measured data. The method herein proposed to ingest GPS observations into the NeQuick model is discussed in the second section of this paper. That section encompasses four subsections: the first presents the relation that links the TEC to the GPS observations; the second summarizes the main features of the NeQuick model and how it can be used to compute the TEC; the third proposes a parameterization of the NeQuick model in

terms of a set of constant parameters that describes the electron density of the F2 ionospheric peak; and the fourth establishes the equation of observation that connects the previously mentioned parameters with the GPS observations and explains how those parameters can be estimated from the data. In the third section of this paper, we apply the method previously described to ingest GPS observations into the NeQuick model and we assess the achieved improvements by comparing our results to Digisonde measurements. Finally, we close the paper with our conclusions.

## 2. Method

### 2.1. Link Between GPS Observations and Slant TEC

[6] Different ionospheric observables can be obtained from the dual-frequency GPS observations as discussed in the literature [e.g., *Manucci et al.*, 1999, and references therein]. The so-called geometry-free linear combination of carrier phase (or P-code observations) in both frequencies provides information related to the slant TEC, *STEC*, along the signal raypath from a satellite at the point $P^S$, to the receiver at the point $P_R$, for the observation at time $t$. This combination is obtained subtracting simultaneous observations in both frequencies, thus removing the satellite-receiver geometrical range and any other frequency-independent biases,

$$\phi_4\left(P_R, P^S, t\right) = \phi_1\left(P_R, P^S, t\right) - \phi_2\left(P_R, P^S, t\right)$$
$$= \alpha \cdot STEC\left(P_R, P^S, t\right)$$
$$+ \beta_R + \beta^S + \beta_R^S + \nu', \qquad (1)$$

where $\phi_4$ is the geometry-free linear combination of the dual-frequency carrier phase observations, $\phi_1$ and $\phi_2$,

**Table 1.** GPS Stations and Days Processed in This Work

| Equinoxes | | | Solstices | | |
|---|---|---|---|---|---|
| Day | Month | Stations | Day | Month | Stations |
| 18 | 03 | CASC-SFER-VILL | 01 | 01 | CASC-SFER-VILL |
| 19 | 03 | CASC-SFER-VILL | 02 | 01 | CASC-SFER-VILL |
| 20 | 03 | CASC-SFER-VILL | 03 | 01 | CASC-SFER-VILL |
| 21 | 03 | CASC-SFER-VILL | 04 | 01 | CASC-SFER-VILL |
| 22 | 03 | CASC-SFER-VILL | 05 | 01 | CASC-SFER-VILL |
| 05 | 10 | CASC-SFER-VILL | 16 | 07 | CASC-SFER-MAD2 |
| 06 | 10 | CASC-SFER-VILL | 17 | 07 | CASC-SFER-MAD2 |
| 07 | 10 | CASC-SFER-VILL | 18 | 07 | CASC-SFER-MAD2 |
| 08 | 10 | CASC-SFER-VILL | 19 | 07 | CASC-SFER-MAD2 |
| 09 | 10 | CASC-SFER-VILL | 20 | 07 | CASC-SFER-MAD2 |
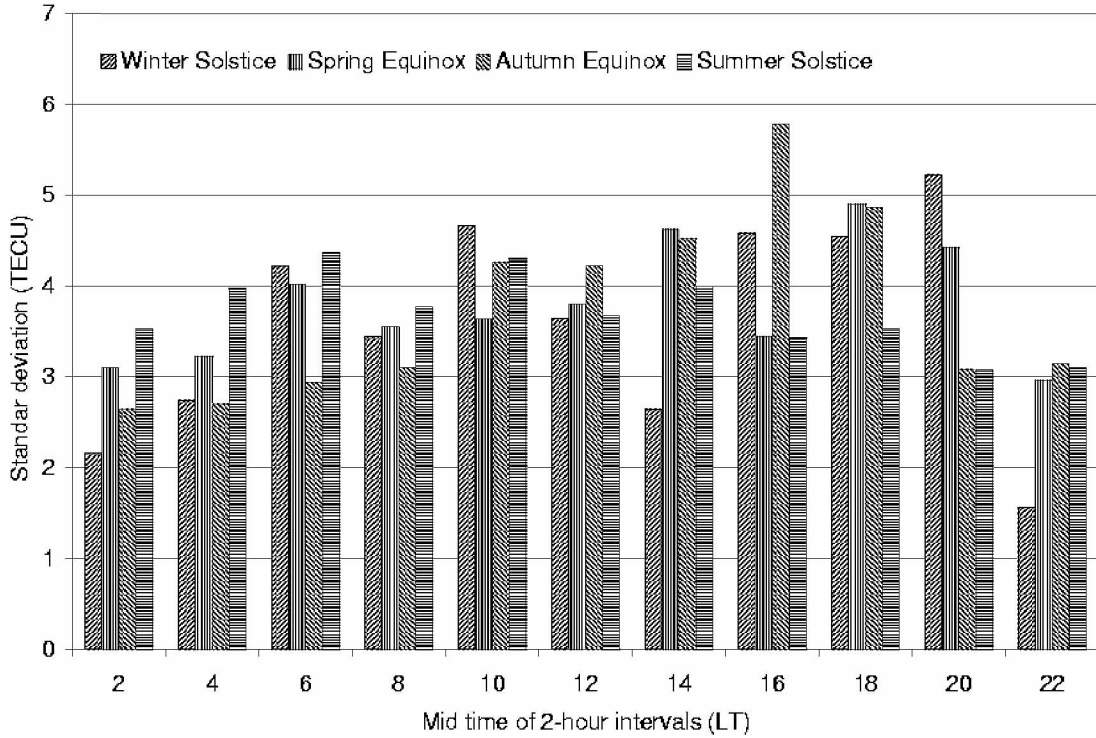
**Figure 2.** Standard deviation of the residuals after solving the linear systems for every 2-hour intervals by least squares. The bars represent the average of the standard deviations of the five days corresponding to each one of the four seasons.

and $STEC$ is the integral of the electron density, $N$, along the signal raypath from the satellite to the receiver,

$$STEC(P_R, P^S, t) = \int_{P_R}^{P^S} N \cdot ds. \qquad (2)$$

$STEC$ is usually measured in TEC Units (TECU), 1 TECU being equivalent to $10^{16}$ electrons per square meter; if the geometry-free combination, $\phi_4(P_R, P^S, t)$, is given in meters, then $\alpha = 0.109$ m/TECU. The other terms in equation (1) are the so-called differential code biases (DCBs) due to frequency-dependent delays produced by the hardware of the receiver and the satellite, $\beta_R$ and $\beta^S$ respectively; the combination of the carrier phase ambiguities in both frequencies, $\beta_R^S$; and the observational error after the combination of the dual-frequency observations, $\nu'$.

[7] An equation analogous to equation (1) can be written for P-code observations. P-code data have the advantage of not being affected by ambiguities, but they have the great disadvantage that the observational error is almost 100 times greater than for carrier-phase observa-

tions. By "leveling" the carrier phase geometry-free combination to the corresponding P-code combination [*Manucci et al.*, 1999], the ambiguity term $\beta_R^S$ can be estimated and removed from equation (1). This task can be done in a preprocessing stage using the following procedure: first, jumps in the carrier phase observations are detected and the data are grouped in continuous arcs; then, a $\beta_R^S$ value for every continuous arc is estimated by averaging the differences between the carrier phase and the P-code geometry-free combinations; finally, the averaged difference is subtracted from the carrier phase observations. In this way, every continuous arc of carrier phase observations is "leveled" (on average) to the P-code observations and the ambiguities are removed from the problem.

[8] Further, satellite and receiver DCBs are also reduced from equation (1), thus obtaining unambiguous (i.e., phase ambiguities removed) and calibrated $S\tilde{T}EC$ data

$$S\tilde{T}EC(P_R, P^S, t) = (\phi_4(P_R, P^S, t) - \beta_R^S - \beta_R - \beta^S)/\alpha$$
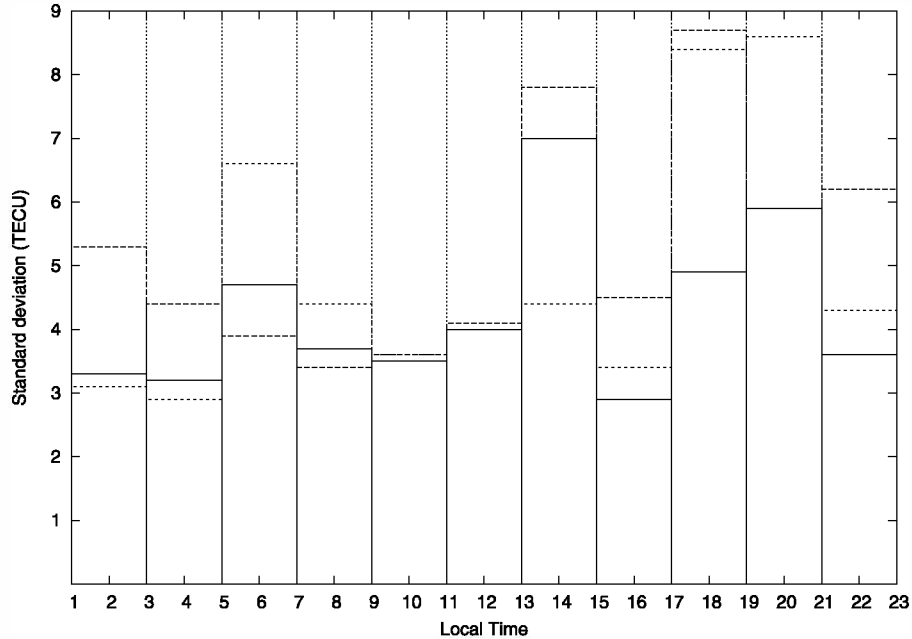$$= STEC(P_R, P^S, t) + v, \qquad (3)$$

**Figure 3.** Standard deviation of the residuals after solving by least squares the linear systems (equation (13)) for every 2-hour interval of March 18, 1999. The lines represent the three solutions found using (a) the ITU-R values, $h_mF2_0$ (solid lines); (b) the $h_mF2_0$ values plus a 10% error (dashed lines); and (c) the $h_mF2_0$ values minus a 10% error (dotted lines).

where $\nu = \nu'/\alpha$ is the observational error scaled by the constant $\alpha$ and hence expressed in TECU. Ambiguities, $\beta_R^S$, and DCBs, $\beta_R$ and $\beta^S$, used in this work have been estimated by means of the La Plata Ionospheric Model as described by *Brunini et al.* [2003, 2005]. The precision in the calibrated experimental STEC determined with GPS can be deduced from *Ciraolo et al.* [2006]; in the better case, the error is $\pm 1.5$ TECU ($1\sigma$), and can be up to $\pm 3$ TECU ($1\sigma$), depending on the receiver/antenna configuration.

## 2.2. Representation of the STEC in Terms of the NeQuick Model

[9] Several empirical models are currently used to describe the electron density distribution in the ionosphere. Among them, the NeQuick model [*Hochegger et al.*, 2000; *Radicella and Leitinger*, 2001; *Leitinger et al.*, 2001] computes the electron density as a function of solar activity, month, UT, height and geographic coordinates. It is a quick-run model for trans-ionospheric applications that allows calculating VTEC or STEC for any specified path through the ionosphere. From 100 km up to the F2 peak this model uses a modified Di Giovanni and Radicella profile formulation [*Di Giovanni and Radicella*, 1990] that includes five semi-Epstein

layers with modeled thickness parameters. This formulation is based on anchor points defined by the critical frequencies f0E, f0F1 and f0F2 of the corresponding ionospheric layers and by the propagation factor, M(3000)F2. NeQuick applies the diffusive equilibrium concept in a topside formulation that is based on a semi-Epstein layer governed by an empirically determined height-dependent scale factor. The model has been adopted by the European Space Agency for satellite navigation applications and has been recommended by the Radioscience Section of the International Telecommunication Union (ITU-R). NeQuick source code is available at http://www.itu.int/ITU-R/study-groups/software. The data files needed are: (a) The ITU-R (CCIR) maps to determine f0F2 and M(3000)F2. They are twelve ASCII files, number 11 for January, number 22 for December (input files ccir11.asc ... ccir22.asc); (b) The monthly average values of the solar activity in terms of the average sunspot number R12 (input file R12.dat); (c) Since the inclination of the geomagnetic induction vector (Dip) is also used by NeQuick submodels, and to be consistent with the ITU-R (CCIR) maps, the limited spherical harmonics expansion for 1977 was used to calculate a grid point map of dip latitude (input file diplats.asc). NeQuick calculates dip latitude by a third order interpolation in geographic latitude and longitude. Dip is calcu-
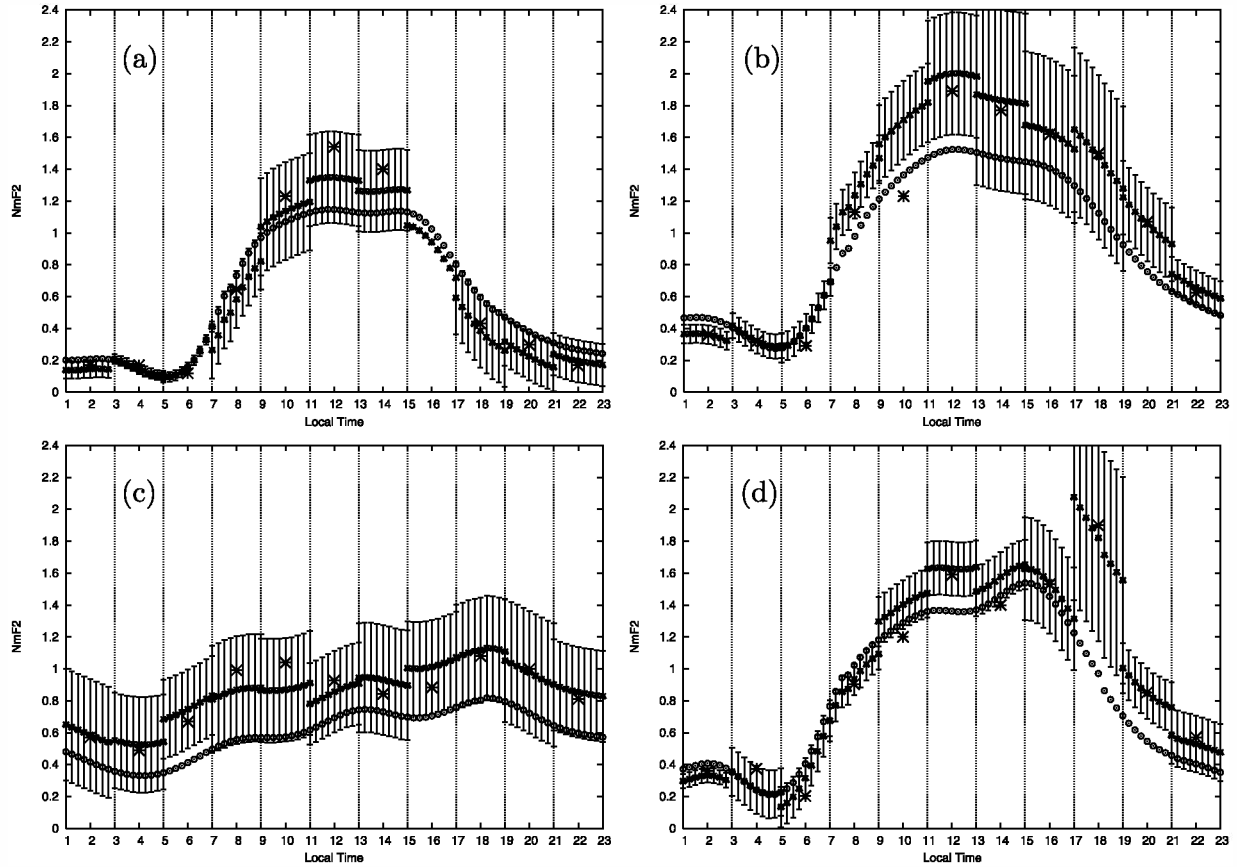
**Figure 4.** Electron density of the F2 peak in units of $10^{12}$ m$^{-3}$ at Arenosillo with a time interval of 15 min along one day. One representative day of each processed month was chosen: (a) January 4, (b) March 18, (c) July 16, and (d) October 6. Crossed solid triangles represent the values of $N_mF2$ found in this work; their error bars $\pm\sigma$ are also plotted. Open circles represent the ITU-R values $N_mF2_0$; and the stars correspond to the Digisonde (true) values $N_mF2_D$. The grid shows the 2-hour intervals used to find $N_mF2$.

lated from dip latitude. All these input files and further details about the NeQuick model are also available in the web site mentioned.

[10] NeQuick describes the electron density distribution $N$ in a given point $P$ of coordinates ($\lambda$, $\varphi$, $h$), and for any time $t$, by a function that primarily depends on the electron density of the F2 peak, $N_mF2$, and the height $h_mF2$ of the peak of the profile, among other parameters. Since these quantities vary with latitude, longitude and time, we can write

$$N = f(P, t; N_mF2(p,t), h_mF2(p,t)), \qquad (4)$$

where $p(\lambda, \varphi)$ is the projection of $P(\lambda, \varphi, h)$ on the Earth surface.

[11] After equations (2) and (4) follows

$$STEC(P_R, P^S, t)$$
$$= \int_{P_R}^{P^S} f(P, t; N_mF2(p,t), h_mF2(p,t)) \cdot ds. \qquad (5)$$

### 2.3. Parameterization of the NeQuick Model

[12] To be able to ingest GPS observations into the NeQuick model, we should develop an adequate mathematical strategy. As we have already said, NeQuick is primarily driven by two parameters, $N_mF2$ and $h_mF2$, the values of which are usually computed as functions of
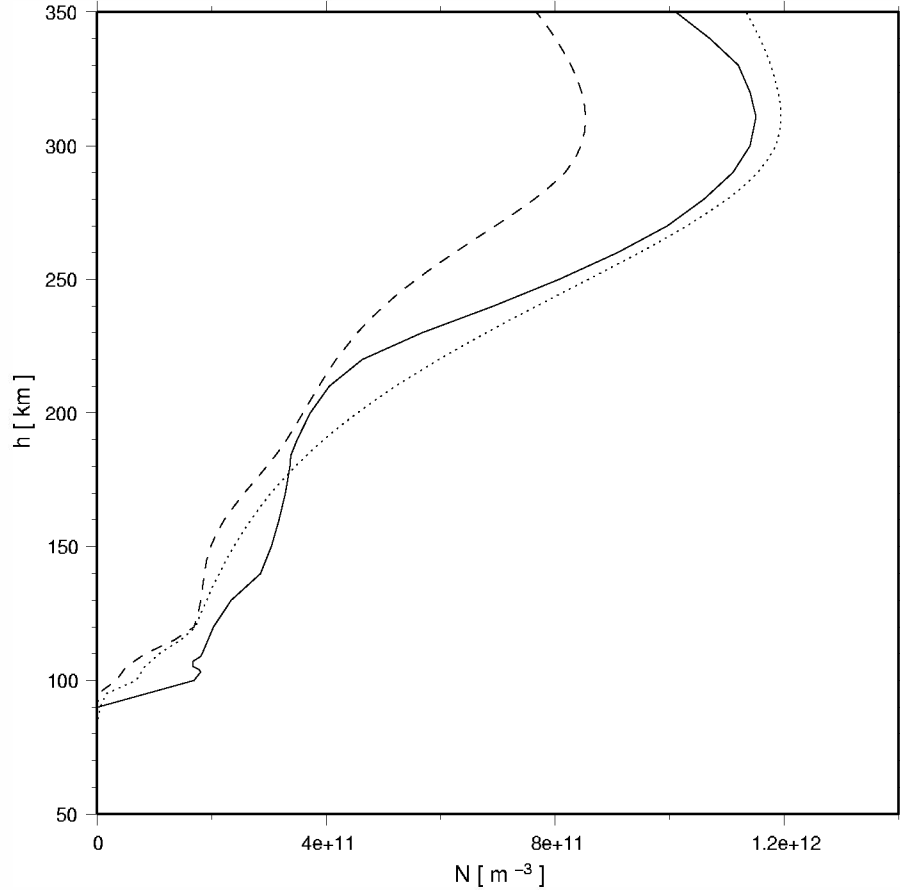
**Figure 5.** Scaled vertical profile of electron density measured by the Digisonde (solid line) and the corresponding profiles computed using NeQuick with the corrected (dotted line) and the ITU-R (dashed line) values of $N_mF2$. Profiles correspond to July 19, 1999, 14 LT at El Arenosillo.

latitude, longitude and time using the ITU-R climatologic database [*Comité Consultatif International des Radiocommunications*, 1967] (and later revisions). Since ITU-R provides monthly averaged values of $N_mF2$ and $h_mF2$, part of the deviation between the STEC measured by GPS and predicted by NeQuick can be attributed to discrepancies between the actual values of these parameters and their monthly average. Therefore, it seems feasible to look for a corrective function to the ITU-R monthly averaged values that improve the agreement between measured and computed STEC, that is

$$N_mF2(p,t) = N_mF2_0(p,t) + \Delta N_mF2(p,t),$$
$$h_mF2(p,t) = h_mF2_0(p,t) + \Delta h_mF2(p,t), \qquad (6)$$

where the left-hand sides are the corrected values and the right-hand sides are the sum of the monthly averaged

values provided by ITU-R and the corresponding correction.

[13] In order to make use of the corrected values we approximate equation (4) by the linear expansion

$$N \cong N_0 + N'_{N0} \cdot \Delta N_mF2(p,t) + N'_{h0} \cdot \Delta h_mF2(p,t), \qquad (7)$$

where

$$N_0 = f(P,t; N_mF2_0(p,t), h_mF2_0(p,t)),$$
$$N'_{N0} = \frac{\partial f}{\partial N_mF2}(P,t; N_mF2_0(p,t), h_mF2_0(p,t)),$$

and

$$N'_{h0} = \frac{\partial f}{\partial h_mF2}(P,t; N_mF2_0(p,t), h_mF2_0(p,t)) \qquad (8)$$

are the electron density function and its derivatives with respect to the electron density and the height of the F2 peak, all evaluated using the ITU-R monthly averages.

[14] In order to compute the derivatives on equation (8) we cut down the NeQuick formulation by considering only the F2 layer and simplifying several mathematical relations. We performed a careful analysis in order to ensure that these simplifications do not affect the results that will be presented later in this paper.

[15] Finally, replacing equation (7) into equation (5) and equation (4), we get the equation that links the STEC and the correction:

$$STEC\left(P_R, P^S, t\right) \cong \int_{P_R}^{P^S} N_0 \cdot ds$$

$$+ \int_{P_R}^{P^S} N'_{N0} \cdot \Delta N_m F2(p, t) \cdot ds$$

$$+ \int_{P_R}^{P^S} N'_{h0} \cdot \Delta h_m F2(p, t) \cdot ds. \qquad (9)$$

## 2.4. Setting Up the Observation Equation System

[16] Hereafter we will restrict our attention to a relatively small region that extends a few hundred kilometers around a point of coordinates $\varphi_0$ and $\lambda_0$ at midionospheric latitude and we will restrict the study to quiet geomagnetic conditions. These restrictions allow us to assume that the corrective function $\Delta N_m F2(p, t)$ should vary smoothly both in space and time. Hence, we propose to represent the spatial variation with a simple bilinear expansion dependent on the latitude, $\varphi$, and the longitude, $\lambda$, of the point $p$, that is

$$\Delta N_m F2(p, t) = X_1 + X_2 \cdot (\lambda - \lambda_0) + X_3 \cdot (\varphi - \varphi_0),$$
$$(10a)$$

where $X_1$, $X_2$, and $X_3$ are coefficients whose values will be taken as constant for a relatively short period of time, $\Delta t$, no longer than 2 hours. On the other hand, the height of the F2 peak, $h_m F2$, was kept equal to the IRU-R value; therefore,

$$\Delta h_m F2(p, t) = 0. \qquad (10b)$$

The previous equation can be justified taking into account that the variation of the electron density with respect to $h_m F2$ has to be integrated along the signal path. In our case, this path is defined by the ground GPS stations and the satellite positions. The coefficient of the $h_m F2$ correction (equation (9)) is the integral of the derivative with respect of the $h_m F2$. This derivative is positive on the bottom side and negative on the topside. So, the numerical integration along the signal path achieves too small values compared with the integration of the derivative with respect to $N_m F2$.

[17] From equations (9), (10a) and (10b) follows, renaming $N'_{N0}$ as $N'_0$,

$$STEC\left(P_R, P^S, t\right) = \int_{P_R}^{P^S} N_0 \cdot ds + X_1$$

$$\cdot \int_{P_R}^{P^S} N'_0 \cdot ds + X_2$$

$$\cdot \int_{P_R}^{P^S} N'_0 \cdot (\lambda - \lambda_0) \cdot ds + X_3$$

$$\cdot \int_{P_R}^{P^S} N'_0 \cdot (\varphi - \varphi_0) \cdot ds. \qquad (11)$$

Note that the first term of the right hand side is just the STEC computed from the ITU-R monthly averaged values, whereas the rest are corrective terms.

[18] Replacing equation (11) into equation (3), we obtain the observation equation of the problem that links the observations and the unknown parameters of the problem, that is

$$S\tilde{T}EC\left(P_R, P^S, t\right) - \int_{P_R}^{P^S} N_0 \cdot ds = X_1 \cdot \int_{P_R}^{P^S} N'_0 \cdot ds$$

$$+ X_2 \cdot \int_{P_R}^{P^S} N'_0 \cdot (\lambda - \lambda_0) \cdot ds$$

$$+ X_3 \cdot \int_{P_R}^{P^S} N'_0 \cdot (\varphi - \varphi_0) \cdot ds + \nu. \quad (12)$$

The left-hand side of equation (12) contains values that are known, i.e., the observed and the computed STEC, while the left hand side contains computable coefficients (i.e., the integrals) that multiply the unknown parameters $X_1$, $X_2$ and $X_3$.

[19] Let us now assume that there are a number of GPS receivers spread on the region under consideration that during the period $\Delta t$ collect $m \gg 3$ observations. After equation (12), the following superabundant linear system of equation of observations can be formed

$$
\begin{pmatrix} a_{11} & a_{12} & a_{13} \\ \vdots & \vdots & \vdots \\ \vdots & \vdots & \vdots \\ a_{m1} & a_{m2} & a_{m3} \end{pmatrix} \cdot \begin{pmatrix} X_1 \\ X_2 \\ X_3 \end{pmatrix} = \begin{pmatrix} b_1 \\ \vdots \\ \vdots \\ b_m \end{pmatrix} + \begin{pmatrix} \nu_1 \\ \vdots \\ \vdots \\ \nu_m \end{pmatrix},
$$

(13)

where

$$
a_{j1} = \left| \int_{P_R}^{P^S} N_0' \cdot ds \right|_j ;
$$

$$
a_{j2} = \left| \int_{P_R}^{P^S} N_0' \cdot (\lambda - \lambda_0) \cdot ds \right|_j ;
$$

$$
a_{j3} = \left| \int_{P_R}^{P^S} N_0' \cdot (\varphi - \varphi_0) \cdot ds \right|_j ; \text{ and}
$$

$$
b_j = \left| S\tilde{T}EC(P_R, P^S, t) - \int_{P_R}^{P^S} N_0 \cdot ds \right|_j ;
$$

$$
j = 1, 2, \ldots, m.
$$

(14)

In order to compute the integrals of equation (14) we have to parameterize the signal raypath, which can be represented by a straight segment from the ground-based receiver at point $P_R$ to the satellite at point $P^S$. Since the electron density described by NeQuick is negligible below $R_l = 60$ km $+ R_E$ and above $R_u = 1000$ km $+ R_E$ ($R_E$ being the Earth's radius), we reduce the integral to the segment lying between the points $P_l(x_l, y_l, z_l)$ and $P_l(x_u, y_u, z_u)$, defined by the intersections of the signal raypath with geocentric spheres of radius $R_l$ and $R_u$, respectively. The parametric equation of this segment is

$$
\frac{x - x_l}{x_u - x_l} = \frac{y - y_l}{y_u - y_l} = \frac{z - z_l}{z_u - z_l} = \omega, 0 \leq \omega \leq 1. \quad (15)
$$

The approximated coordinates of a given point $P(\varphi, \lambda, h) \equiv P(\varphi(\omega), \lambda(\omega), h(\omega))$ in the segment from $P_l$ to $P_u$

can be written in terms of the previously defined parameterization as

$$
\lambda(\omega) = \tan^{-1} \left( \frac{\psi \cdot \omega + y_l}{\xi \cdot \omega + x_l} \right),
$$

$$
\varphi(\omega) = \tan^{-1} \left( \frac{\zeta \cdot \omega + z_l}{\sqrt{(\xi \cdot \omega + x_l)^2 + (\psi \cdot \omega + y_l)^2}} \right),
$$

$$
h(\omega) = \sqrt{(\xi \cdot \omega + x_l)^2 + (\psi \cdot \omega + y_l)^2 + (\zeta \cdot \omega + z_l)^2},
$$

(16)

where $\xi = x_u - x_l$, $\psi = y_u - y_l$ and $\zeta = z_u - z_l$.

[20] Therefore the explicit expressions for the equation (14) integrals are

$$
\int_{P_R}^{P^S} N_0 \cdot ds = \int_0^1 f(P, t; N_m F2_0(p, t), h_m F2_0(p, t))
$$
$$
\cdot \sqrt{\xi^2 + \psi^2 + \zeta^2} \, d\omega,
$$

$$
\int_{P_R}^{P^S} N_0' \cdot ds = \int_0^1 \frac{\partial f}{\partial N_m F2}(P, t; N_m F2_0(p, t), h_m F2_0(p, t))
$$
$$
\cdot \sqrt{\xi^2 + \psi^2 + \zeta^2} \, d\omega,
$$

$$
\int_{P_R}^{P^S} N_0' \cdot (\lambda - \lambda_0) \cdot ds = \int_0^1 (\lambda(\omega) - \lambda_0)
$$
$$
\cdot \frac{\partial f}{\partial N_m F2}(P, t; N_m F2_0(p, t),
$$
$$
\cdot h_m F2_0(p, t))
$$
$$
\cdot \sqrt{\xi^2 + \psi^2 + \zeta^2} \, d\omega,
$$

$$
\int_{P_R}^{P^S} N_0' \cdot (\varphi - \varphi_0) \cdot ds = \int_0^1 (\varphi(\omega) - \varphi_0)
$$
$$
\cdot \frac{\partial f}{\partial N_m F2}(P, t; N_m F2_0(p, t),
$$
$$
\cdot h_m F2_0(p, t))
$$
$$
\cdot \sqrt{\xi^2 + \psi^2 + \zeta^2} \, d\omega, \quad (17)
$$

where $P(\varphi, \lambda, h) \equiv P(\varphi(\omega), \lambda(\omega), h(\omega))$, $p(\varphi, \lambda) \equiv p(\varphi(\omega), \lambda(\omega))$ and $\sqrt{\xi^2 + \psi^2 + \zeta^2} d\omega = ds$. The functions to be
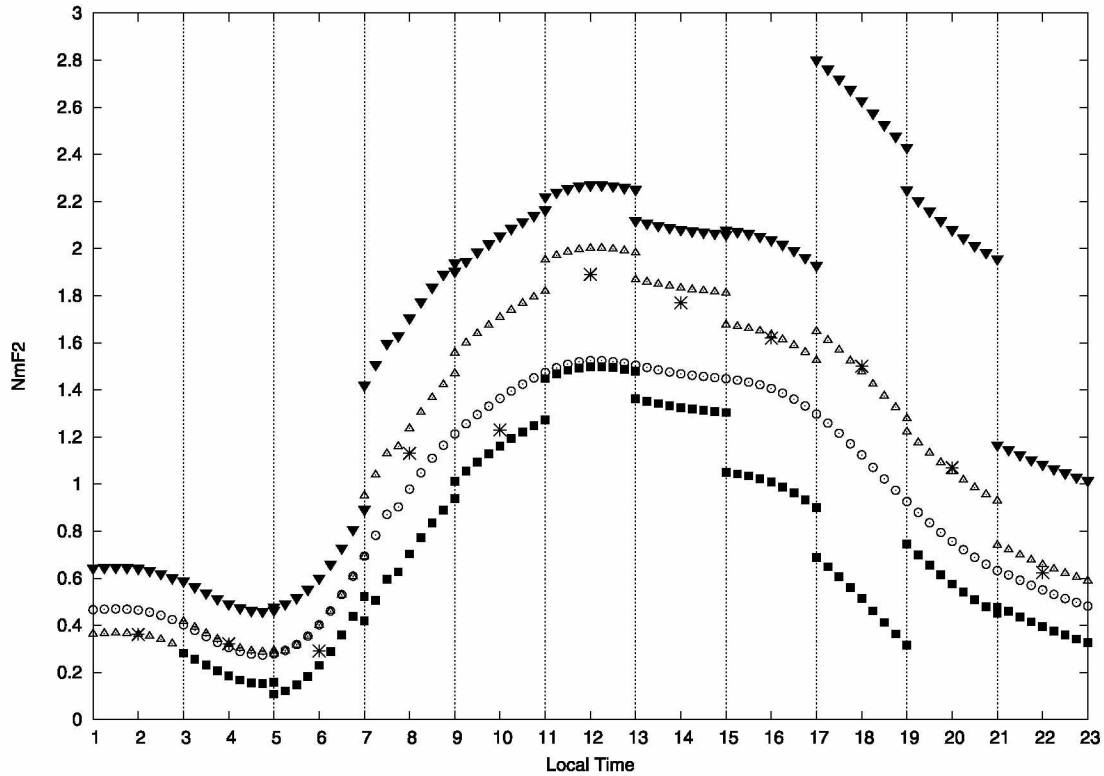
**Figure 6.** Electron density of the F2 peak in units of $10^{12}$ m$^{-3}$ at Arenosillo with a time interval of 15 min along March 18, 1999. Open triangles represent the values of $N_mF2$ we found using $h_mF2_0$; circles correspond to the ITU-R values $N_mF2_0$; stars are the Digisonde (true) values $N_mF2_D$; squares correspond to the $N_mF2$ values obtained using $h_mF2_0$ plus a 10% error; and solid triangles represent the values of $N_mF2$ found using $h_mF2_0$ minus a 10% error. The grid shows the 2-hour intervals used to find the new values of the electron density of the F2 peak.

integrated are smooth and free of discontinuities in the integration domain; this allowed us to integrate them fast and reliably by using a third order Gauss algorithm, with successive subdivisions of the interval until a relative tolerance between subdivisions of $10^{-3}$ was achieved.

## 3. Results

[21] In order to investigate the applicability of the above described procedure we used actual GPS observations from three ground-based receivers located in the Spanish Peninsula, all belonging to the IGS network. As Figure 1 shows, the receivers are located in the vertex of an almost equilateral triangle with sides of approximately 500 kilometers. Thus, $\lambda_0$ and $\varphi_0$ are the coordinates of the baricenter of the observing network. We processed twenty complete days arranged in four groups of five days, each one close to solstices and equinoxes of the year 1999. All these days correspond to medium-high solar activity and quiet geomagnetic conditions. Table 1

summarizes the GPS stations and days processed to obtain the results that will be presented in this section. Moreover to crosscheck our results, we used ionograms recorded by a ground-based Digisonde at El Arenosillo, Spain (37.1 N; 353.2 E; modip = 45.5) (see Figure 1). Those ionograms were scaled using the procedure described by *Reinisch and Huang* [1983] and *Reinisch* [1996]. Digisondes directly measure $N_mF2$ since

$$N_mF2\left[cm^{-3}\right] = \frac{1}{80.6}\left(f_0F2[MHz]\right)^2, \qquad (18)$$

where $f_0F2$ is the measured critical frequency of the F2 layer. The corresponding peak height is obtained from the true height inversion program [*Huang and Reinisch*, 1996], which allows to calculate the bottom-side electron density profiles.

[22] Firstly, we computed unambiguous and calibrated *STEC* data from the GPS observations, as stated in

**Table 2.** Average of the Absolute Value of the Relative Errors for the Five Days That Represent Each One of the Four Seasons

| | Solstices | | | | Equinoxes | | | |
| | Winter | | Summer | | Spring | | Fall | |
| Local Time | $\varepsilon_{rel}$ | $\varepsilon_{rel,0}$ | $\varepsilon_{rel}$ | $\varepsilon_{rel,0}$ | $\varepsilon_{rel}$ | $\varepsilon_{rel,0}$ | $\varepsilon_{rel}$ | $\varepsilon_{rel,0}$ |
|---|---|---|---|---|---|---|---|---|
| 2 | 0.13 | 0.36 | 0.20 | 0.46 | 0.06 | 0.11 | 0.06 | 0.10 |
| 4 | 0.13 | 0.17 | 0.17 | 0.49 | 0.13 | 0.22 | 0.22 | 0.39 |
| 6 | 0.22 | 0.25 | 0,17 | 0.32 | 0,24 | 0.21 | 0.39 | 0.48 |
| 8 | 0.20 | 0.28 | 0.10 | 0.31 | 0.25 | 0.12 | 0.07 | 0.07 |
| 10 | 0.16 | 0.24 | 0.09 | 0.29 | 0.25 | 0.17 | 0.10 | 0.08 |
| 12 | 0.13 | 0.17 | 0.03 | 0.18 | 0.06 | 0.20 | 0.12 | 0.12 |
| 14 | 0.07 | 0.26 | 0.08 | 0.31 | 0.06 | 0.31 | 0.16 | 0.09 |
| 16 | —— | —— | 0.08 | 0.29 | 0.06 | 0.27 | 0.03 | 0.14 |
| 18 | 0.54 | 0.57 | 0.03 | 0.27 | 0.09 | 0.33 | 0.07 | 0.34 |
| 20 | 0.20 | 0.67 | 0.07 | 0.15 | 0.07 | 0.24 | 0.07 | 0.15 |
| 22 | 0.12 | 1.12 | 0.07 | 0.30 | 0.12 | 0.17 | 0.05 | 0.15 |

equation (3); as it was already mentioned, we estimated the ambiguities and DCBs for satellites and receivers using the La Plata Ionospheric Model [*Brunini et al.*, 2003, 2005]. Then, we grouped the observations in intervals of 2 hours and computed a superabundant linear system of equation of observations (equation (13)) for every 2-hour interval. We solved these systems by applying the least squares method and estimated the constant parameters $X_1$, $X_2$ and $X_3$ of equation (10a) for every 2-hour interval.

[23] In order to get a first assessment of the quality of the results, we computed the residuals, $\nu_1, \ldots, \nu_m$, for every observation equation system and the corresponding standard deviation, $\sigma = \sqrt{\sum_{j=1}^{m} \nu_j^2 / (m - 3)}$. The obtained results are summarized in Figure 2, where we plotted the average of the standard deviations of the five days that represent each one of the four seasons. It can be appreciated that no value exceeds from ±6 TECU, which is considered a quite encouraging result. After *Meza et al.* [2002], we know that empirical ionospheric models driven by climatological parameters are affected by errors larger than the ±6 TECU found in this work. The individual residuals do not show systematic behaviors, they seem to be similar for either solstices or equinoxes and they tend to reach slightly higher values in the afternoon, from about 15 to 19 LT. Besides, the typical errors on the STEC, or DCBs, do not greatly affect the results, because they compensate when including all the observed satellites in the computation. On the other hand, one may wonder whether a nonfixed $h_mF2$ would have reduced the residuals. According to what was said in justifying equation (10b), this is not the case: the variation of the $h_mF2$ parameter will not significantly affect the residuals when only ground-based GPS data are used. To confirm this, we have reproduced the computation with an added 10% error in $h_mF2_0$ and also with a subtracted 10% error in $h_mF2_0$. As an example, Figure 3 shows, for a particular day and in 2-hour intervals, the new values of the standard deviations obtained for both cases along with the value obtained originally. The figure reveals that the differences are within an acceptable tolerance. Nevertheless, we must take into account, as we will see below, that the value of $h_mF2$ will affect the results in the adjustment of $N_mF2$.

[24] Next, we used equations (10a) and (10b) and the previously estimated parameters, $X_1$, $X_2$ and $X_3$, to evaluate the corrective function $\Delta N_mF2(p, t)$, and then equation (6) to evaluate the corrected function $N_mF2(p, t)$. In Figure 4 we represented the corresponding $N_mF2(p, t)$ found for each 2-hour interval at Arenosillo with a time interval of 15 min along one day. We plotted the values of $N_mF2$, their errors $\pm\sigma$, and $N_mF2_0$, along with the values observed by the Digisonde as a reference for one representative day of each month processed. From these plots, we can see that, overall, there is an improvement in the values; moreover, almost all the real (Digisonde) data pass through the error bars ($\pm\sigma$), the few that do not falling comfortably into a $3\sigma$ band. The errors $\sigma$ were computed as follows. According to equation (6), the error in $N_mF2$ is a combination of both the error in $N_mF2_0$ and the error in $\Delta N_mF2$. The first was estimated as a monthly mean (at a given hour) with respect to the real value. The second one was computed from the propagation of errors generated by equation (10a), using the covariance matrix obtained in the solution of the system of equation (13). Once computed, the errors in $\Delta N_mF2$ resulted negligible with respect to the errors in $N_mF2_0$, yielding a error in $N_mF2$ almost independent of the error in $\Delta N_mF2$. Figure 6 shows that the errors have a uniform distribution in July, whereas in the rest of the cases, there are small errors at the beginning of the day, which start to grow at noon, and decrease again at night. Also, the maximum values of the errors in January are similar to those of July, whereas the maxima in October and March are even greater. On the other hand, it is worth to note that the discontinuities in $N_mF2$ between different 2-hour intervals simply reflect that solutions were obtained spanning only those 2-hour intervals, each interval having its own solution. This was done because our approximation (equation (6)) is only valid for a short period of time. Should continuous values be required along the day, the curve must be smoothed, e.g., with splines or even finding solutions using the values of each previous interval.

[25] Just to give an example, Figure 5 compares the scaled vertical profile of electron density measured by the Digisonde and the corresponding profiles computed using the NeQuick model. The comparison was limited to the bottom-side profile because the Digisonde does not provide measurements above the F2 peak. Two different profiles were computed from NeQuick: one
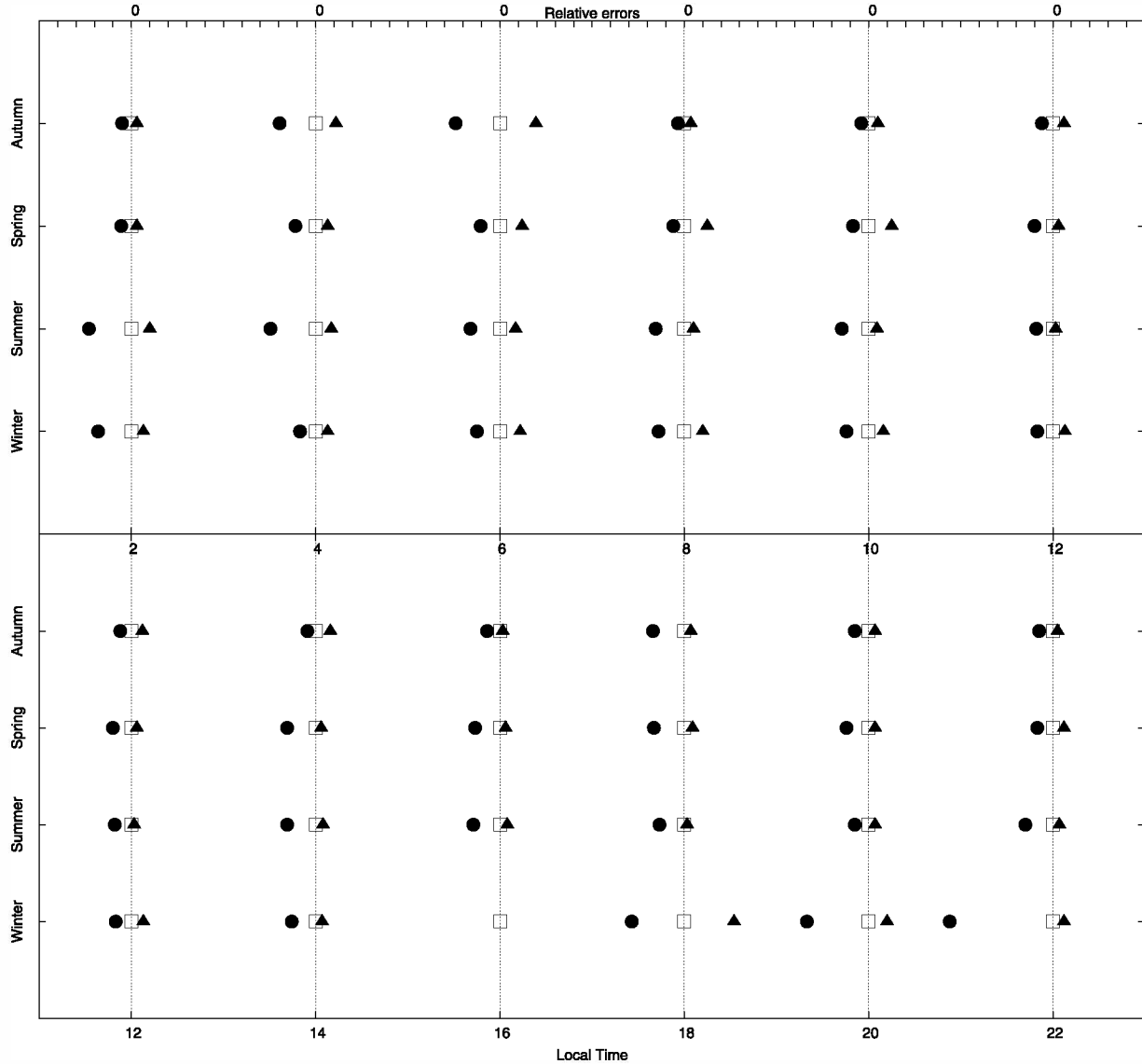
**Figure 7.** Five-day average for the different seasons of the absolute values of the relative error of the corrected and the ITU-R values of $N_mF2$ taking as a reference the value inferred from Digisonde measurements at Arenosillo, Spain, for every midpoint of the 2-hour intervals, $\varepsilon_{rel}$ and $\varepsilon_{rel,0}$, respectively. A square indicates a particular season at a particular local time and corresponds to $\varepsilon_{rel} = \varepsilon_{rel,0} = 0$. At its right (solid triangle) and left (solid circle) the values of $\varepsilon_{rel}$ and $\varepsilon_{rel,0}$, respectively, were plotted. The top axis x2 indicates the scale of these relative errors; ticks are separated by 0.2.

using the corrected function, $N_mF2(p_D, t_0)$, $p_D$ representing the Digisonde latitude and longitude and $t_0$ the midtime of every 2-hour interval; and the other using the climatological value, $N_mF2_0(p_D, t_0)$, computed from the ITU-R database. Both profiles were computed using the height of the F2 peak provided by the ITU-R database. It is apparent that the corrections improve the

general agreement between the electron density computed by NeQuick and measured by the Digisonde. Also, as a consequence of the shifting of the $N_mF2$ value in order to keep the area of the profile provided by the GPS data, the profile shape has changed quite a bit; i.e., below the F2 peak of the former profile, the E and F1 layers stand out, due to their conspicuous hills and valleys, whereas
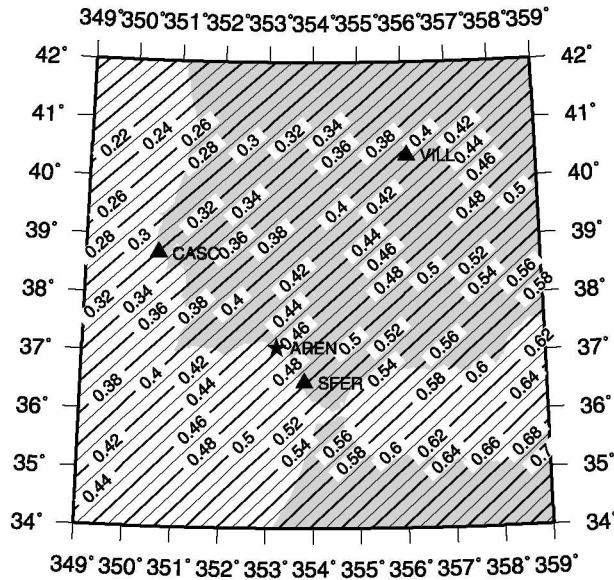
**Figure 8a.** Level curves of $\Delta N_m F2/N_m F2_0$ for the region around the Spanish stations CASC, SFER, and VILL used to compute them. The values correspond to the solstice of January 3, 1999, between 7 AM and 9 AM. The location of the Digisonde at Arenosillo is marked with a star as a reference.

in the new profile, those features are milder. This modification is the "fading out" of the upper semi-Epstein layers for the E and F1 regions in the vicinity of the F2 layer peak to avoid secondary maxima, and ensures that the electron density at the F2 layer peak corresponds exactly to f0F2.

[26] On the other hand, we would like to emphasize the relevance of the fixed value of $h_m F2$ used in order to obtain a good adjustment in $N_m F2$. In this paper, we used the monthly averaged values provided by ITU-R, $h_m F2_0$, which are available at any location at any time. For a particular day, Figure 6 compares the results found for three different values of $h_m F2$: (a) using the monthly averaged values provided by ITU-R, $h_m F2_0$; (b) using $h_m F2_0$ plus a 10% error; and (c) using $h_m F2_0$ minus a 10% error. Case a yielded the best fit. In cases b and c we observe values lesser and greater than those of case a, respectively, since $N_m F2$ adjusts to give the same STEC.

[27] Finally, in order to assess the improvement gained after the data ingestion procedure presented in this paper we compared the errors of the electron density of the F2 peak before and after correction, using as ground truth the value measured by the Digisonde. Specifically, we computed the absolute value of the relative errors defined as $\varepsilon_{rel} = |(N_m F2(p_D, t_0) - N_m F2_D(t_0))/N_m F2_D(t_0)|$ and $\varepsilon_{rel,0} = |(N_m F2_0(p_D, t_0) - N_m F2_D(t_0))/N_m F2_D(t_0)|$,

where $N_m F2_D(t_0)$ is the value obtained from Digisonde measurements. The obtained results are summarized in Table 2 and in its corresponding Figure 7, where we plotted the average of these quantities for the five days that represent each one of the four seasons. The analysis of the plots reveals an overall reduction of the relative error to approximately the half of its original value. For the summer period, the relative error after data ingestion reduces from about 40% to 20% and for the other seasons, reduces from 20–30% to almost 10%. The correction procedure seems to perform better from late afternoon (~14 LT) until early morning (~4 LT), than for the other 2-hour intervals. This is probably due to the fact that the NeQuick model performs rather well during daytime, and its estimations are worst during nighttime [*Miró Amarante et al.*, 2004]. There are a few 2-hour intervals where the procedure does not reduce the relative error, but in all these cases the original error of the tabulated $N_m F2$ with respect to the Digisonde was rather small already before the correction being applied. In addition, the worsening after correction never exceeded from 10%. These unfavorable situations always happened for equinox periods and we suspect that this problem could arouse from inadequacies of the NeQuick topside [*Miró Amarante et al.*, 2004]. In fact, the formulation of this part of the profile is currently under reviewing [*Coïsson et al.*, 2006].

[28] Moreover, our results may be used to improve the ITU-R climatologic database in a geographical limited
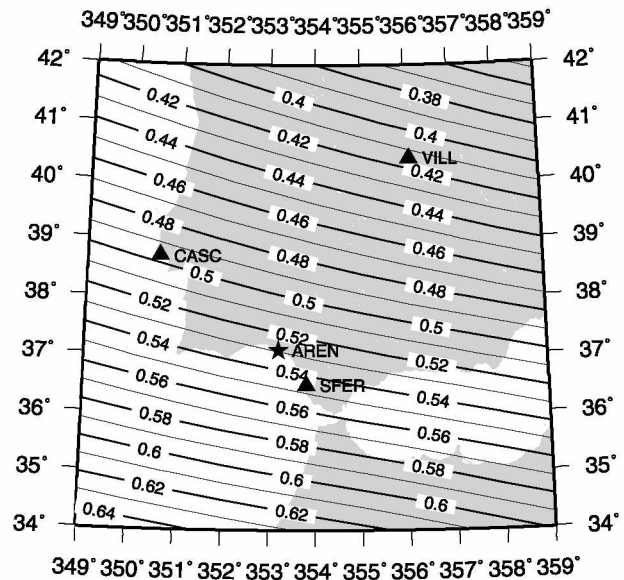


**Figure 8b.** Same as Figure 8a, but the values corresponding to the equinox of October 6, 1999, from 9 PM to 11 PM.

region. This region must be near stations with available data in order to the bilinear correction to be valid. Figures 8a and 8b show an application of this idea. Inspection of similar figures corresponding to all the two-hour intervals of all the days computed revealed that, although the gradient of the corrections is mild in general, the corrections themselves can be significant, like those of Figures 8a and 8b. Moreover, that inspection also showed that there is no apparent pattern in the corrections, i.e., there is no general result applicable to any case.

## 4. Conclusions

[29] We presented a procedure to ingest STEC measured with GPS into the NeQuick ionospheric model. The procedure relies upon improving the parameter that drives the electron density profile described by NeQuick (and by many other empirical models), i.e., the electron density of the F2 peak. To achieve this goal, we parameterized the model as function of that parameter and optimized its value in order to minimize the deviations between computed and measured STEC. We assessed the effectiveness of this procedure in rather benevolent ionospheric conditions, i.e., we applied it in a midlatitude region with an extension of few hundred kilometers and we restricted our analysis to few selected quiet geomagnetic days that cover solstices and equinoxes conditions during a medium-high solar activity year. Under these conditions, the procedure was able to reproduce the observed STEC with an overall agreement better than ±6 TECU. Even for the rather benevolent conditions considered in this work, empirical models are affected by much larger errors than those verified here. We believe, therefore, that data ingestion procedure fairly improves the ability of NeQuick to reproduce the observed STEC.

[30] Always under the conditions imposed to this work, the procedure demonstrated its usefulness to improve the climatological value of the electron density of the F2 peak computed from the ITU-R database. We assessed the ability of our data ingestion procedure to improve this parameter by comparisons against values inferred from Digisonde measurements and we found an overall reduction of the errors to around half of the original values.

[31] Under more stringent conditions (i.e., high solar activity and/or disturbing geomagnetic conditions), the bilinear correction may be insufficient. Also, the temporal resolution of our method (2 hours) may be too large to account for the possible short-time changes that the variables may develop in this case. Thus, this approach has to be taken with caution if it is intended to be applied in those cases.

[32] As a future work, we plan to compare our results with those which would be obtained with other models (including the Chapman model), in order to determine which ones have the better fit to the observed data.

## References

Beutler, G., M. Rotacher, S. Schaer, T. A. Springer, J. Kouba, and R. E. Neilan (1999), The International GPS Service (IGS): an interdisciplinary service in support of earth sciences, *Adv. Space Res.*, *23*(4), 631–653.

Brunini, C., M. A. Van Zele, A. Meza, and M. Gende (2003), Quiet and perturbed ionospheric representation according to the electron content from GPS signals, *J. Geophys. Res.*, *108*(A2), 1056, doi:10.1029/2002JA009346.

Brunini, C., A. Meza, and W. Bosch (2005), Temporal and spatial variability of the bias between TOPEX and GPS derived TEC, *J. Geod.*, *79*(4-5), 175–188.

Ciraolo, L., F. Azpilicueta, C. Brunini, and A. Meza (2006), Calibration errors on experimental slant total electron content (TEC) determined with GPS, *J. Geod.*, doi:10.1007/s00190-006-0093-1.

Coïsson, P., S. M. Radicella, R. Leitinger, and B. Nava (2006), Topside electron density in IRI and NeQuick: features and limitations, *Adv. Space Res.*, *37*(5), 937–942.

Comité Consultatif International des Radiocommunications (1967), CCIR atlas of ionospheric characteristics, Union Int. des Télécommun., Geneva.

Di Giovanni, G., and S. M. Radicella (1990), An analytical model of the electron density profile in the ionosphere, *Adv. Space Res.*, *10*(11), 1127–1130.

Feltens, J. (1998), Chapman profile approach for 3-d global TEC representation, paper presented at Analysis Centers Workshop, Int. GNSS Serv., Darmstadt, Germany, 9 –11 Feb.

Gao, Y., P. Heroux, and J. Kouba (1994), Estimation of GPS receiver and satellite L1/L2 signal delay biases using data from CACS, paper presented at KIS-94, Banff, Canada, 30 Aug. to 2 Sept.

García-Fernández, M., M. Hernandez-Pajares, M. Juan, and J. Sanz (2003), Improvement of ionospheric electron density estimation with GPS-MET occultations using Abel inversion and VTEC information, *J. Geophys. Res.*, *108*(A9), 1338, doi:10.1029/2003JA009952.

Hajj, G. A., R. Ibañez-Meier, E. R. Kursinski, and L. J. Romans (1994), Imaging the ionosphere with the Global Positioning System, *Imaging Syst. Technol.*, *5*, 174–184.

Hajj, G. A., B. D. Wilson, C. Wang, X. Pi, and I. G. Rosen (2004), Data assimilation of ground GPS electron content into a physics-based ionospheric model by use of the Kalman filter, *Radio Sci.*, *39*, RS1S05, doi:10.1029/2002RS002859.

Hernández-Pajares, M. (2003), Performance of IGS ionosphere TEC maps, IGS IONO WG report, 22nd IGS Governing Board, Nice, 6 April.

Hernández-Pajares, M., J. M. Juan, and J. Sanz (1999), New approaches in global ionospheric determination using ground GPS data, *J. Atmos. Sol. Terr. Phys.*, *61*, 1237–1247.

Hernández-Pajares, M., J. Juan, and J. Sanz (2000), Improving the Abel inversion by adding round GPS data to LEO radio occultation inionospheric sounding, *Geophys. Res. Lett.*, *27*(16), 2473–2476.

Hernández-Pajares, M., J. M. Juan, J. Sanz, and D. Bilitza (2002), Combining GPS measurements and IRI model values for space weather specifications, *Adv. Space Res.*, *29*(6), 949–958.

Hochegger, G., B. Nava, S. M. Radicella, and R. Leitinger (2000), A family of ionospheric models for different uses, *Phys. Chem. Earth*, *25*(4), 307–310.

Howe, B. M., K. Runciman, and J. A. Secan (1998), Tomography of the ionosphere: four-dimensional simulation, *Radio Sci.*, *33*, 109–128.

Huang, X., and B. W. Reinisch (1996), Vertical electron density profiles from the Digisonde network, *Adv. Space Res.*, *18*(6), 21–29.

Jakowski, N., A. Wehrenpfennig, S. Heise, C. H. L. Reigber, L. Grunwaldt, and T. K. Meehan (2002), GPS radioocculta-tion measurements of the ionosphere from CHAMP: Early results, *Geophys. Res. Lett.*, *29*(10), 1457, doi:10.1029/2001GL014364.

Komjathy, A., R. B. Langley, and D. Bilitza (1998), Ingesting GPS-derived TEC data into the International Reference Io-nosphere for single frequency radar altimeter ionospheric delay corrections, *Adv. Space Res.*, *22*(6), 793–801.

Leitinger, R., B. Nava, G. Hochegger, and S. M. Radicella (2001), Ionospheric profilers using data grids, *Phys. Chem. Earth*, *26*(5), 293–301.

Mannucci, A. J., B. D. Wilson, D. N. Yuan, C. Ho, U. J. Lindqwister, and T. F. Runge (1998), A global mapping technique for GPS-derived ionospheric total electron content measurements, *Radio Sci.*, *33*, 565–582.

Manucci, A. J., B. A. Iijima, U. J. Lindqwister, X. Pi, L. Sparks, and B. D. Wilson (1999), GPS and ionosphere URSI reviews of Radio Science, Jet Propul. Lab., Pasadena, Calif.

Meza, A. (1999), Three-dimensional ionospheric models from earth and space based GPS observations, Ph.D. thesis, Univ. Nac. de La Plata, La Plata, Argentina.

Meza, A., C. Brunini, and A. Kleusberg (2000), Global iono-spheric models in three dimensions from GPS measure-ments: numerical simulation, *Geofís. Int.*, *39*(1), 21–27.

Meza, A. M., A. R. Díaz, C. Brunini, and M. A. Van Zele (2002), Systematic behavior of semiempirical global iono-spheric models in quiet geomagnetic conditions, *Radio Sci.*, *37*(3), 1037, doi:10.1029/2001RS002482.

Miró Amarante, G., F. Azpilicueta, S. M. Radicella, and C. Brunini (2004), Vertical Topside Total Electron Content comparison of TOPEX data with IRI and NeQuick models, paper presented at International Beacon Satellite Sympo-sium, Abdus Salam ICTP, Trieste, Italy.

Nava, B., P. Coisson, G. Miró Amarante, and S. M. Radicella (2003), A new model assisted method for ionosphere elec-tron density reconstruction, paper presented at Special Sym-posium of the URSI Joint Working Group FG Proceedings, Matera, Italy, Oct.

Radicella, S. M., and R. Leitinger (2001), The evolution of the DGR approach to model electron density profiles, *Adv. Space Res.*, *27*(1), 35–40.

Reinisch, B. W. (1996), Modern ionosondes, in *Modern Iono-spheric Science*, edited by H. Kohl, R. Ruster, and K. Schlegel, pp. 440–458, Eur. Geophys. Soc., Katlenburg-Lindau, Germany.

Reinisch, B. W., and X. Huang (1983), Automatic calculation of electron density profiles from digital ionograms: 3. Pro-ceedings of bottom-side ionograms, *Radio Sci.*, *18*(3), 477–492.

Ruffini, G., L. Cucurull, A. Flores, and A. Rius (1999), APIM-aided Kalman filter for GPS tomography of the ionospheric electron content, *Phys. Chem. Earth*, *24*(4), 365–369.

Schaer, S. (1999), Mapping and predicting the Earth's iono-sphere using the Global Positioning System, Ph.D. thesis, Univ. of Berne, Berne, Switzerland.

───────

C. Brunini, E. Gularte, and A. Meza, Facultad de Ciencias Astronómicas y Geofísicas, Universidad Nacional de La Plata, Buenos Aires 1900, Argentina. (erika@fcaglp.unlp.edu.ar)

P. Coisson, B. Nava, and S. M. Radicella, Aeronomy and Radiopropagation Laboratory, Abdus Salam International Center for Theoretical Physics, 34014 Trieste, Italy.

M. Mosert, Complejo Astronómico El Leoncito, San Juan 5411, Argentina.